Research article

Two-dimensional double horizon peridynamics for membranes

Zhenghao Yang[1], Erkan Oterkus[2,*] and Selda Oterkus[2]

[1] Otto von Guericke University, Universitätspl. 2, Magdeburg 39106, Germany
[2] PeriDynamics Research Centre, Department of Naval Architecture, Ocean and Marine Engineering, University of Strathclyde, 100 Montrose Street, Glasgow G4 0LZ, United Kingdom

* Correspondence: Email: erkan.oterkus@strath.ac.uk; Tel: +44-141-548-3876.

Abstract: In this study, a two-dimensional "double-horizon peridynamics" formulation was presented for membranes. According to double-horizon peridynamics, each material point has two horizons: inner and outer horizons. This new formulation can reduce the computational time by using larger horizons and smaller inner horizons. To demonstrate the capability of the proposed formulation, various different analytical and numerical solutions were presented for a rectangular plate under different boundary conditions for static and dynamic problems. A comparison of peridynamic and classical solutions was given for different inner and outer horizon size values.

Keywords: Peridynamics; double horizon; nonlocal; classical; membrane; two-dimensional

1. Introduction

As a new continuum-mechanics formulation, peridynamics [1] has been introduced by considering the challenges that classical continuum mechanics (CCM) is facing. One major challenge of CCM is discontinuities such as cracks in the solution domain. In this case, spatial derivatives in governing equations of CCM cannot be defined along discontinuities, which makes governing equations. In addition, CCM does not have a length scale parameter, which makes it difficult to make predictions for some emerging areas such as nanoengineering. Peridynamics overcomes the first issue by utilising integrations rather than spatial derivatives in its governing equation. Moreover, by incorporating a length scale parameter, the horizon, it can capture physical behaviours seen at small scales.

There has been a significant development on peridynamics, especially during recent years. Amongst these, De Meo et al. [2] demonstrated the pit-to-crack process using peridynamics, starting from crack initiation to crack propagation phases by considering the microstructural features. Yin et al. [3] used peridynamics for large deformations and hyper-elastic materials. Liu et al. [4] utilized peridynamics to investigate fracture characteristics observed in zigzag graphene sheets. Peridynamics has also been used for the analysis of functionally graded materials [5] and composite materials [6]. Chen et al. [7] developed a fully coupled thermo-mechanical peridynamic formulation to analyse concrete cracking. Qin et al. [8] developed a peridynamic model for hydraulic fracturing of layered rock mass systems. Lakshmanan et al. [9] performed three-dimensional crystal plasticity simulations. Yan et al. [10] developed a coupled water flow and chemical transport peridynamic model suitable for unsaturated porous media. Wang et al. [11] presented a mixed-mode peridynamic fatigue model by employing ordinary-state-based peridynamics. Peridynamic formulations for beam [12,13] and plate [14,15] structures are also available in the literature. Peridynamics has also been utilized to free vibration [16] and buckling [17] analysis of cracked plates.

Although they are limited, analytical solutions to peridynamic equations for some problems are available [18,19]. Numerical implementation of peridynamics is usually based on a meshless approach rather than mesh-based or semi-analytical approaches [20]. Ni et al. [21] coupled the finite element method and ordinary state-based peridynamics. Pagani and Carrera [22] coupled three-dimensional peridynamic formulation and higher-order one-dimensional finite elements. Xia et al. [23] coupled isogeometric analysis and peridynamics for the analysis of cracks. Liu et al. [24] coupled peridynamics and updated Lagrangian particle hydrodynamics to simulate ice–water interactions. Wang et al. [25] developed three-dimensional conjugated bond pair–based peridynamic formulation. Diana et al. [26] introduced anisotropic peridynamics suitable for homogenised micro-structured materials. Mikata [27] presented peridynamic formulations for fluid mechanics and acoustics. Another new peridynamic concept is "peridynamic differential operator", which is mainly used to convert differentiations to their corresponding integral form [28]. Ren et al. [29] developed a higher-order nonlocal operator method for the solution of boundary value problems. In another study, Ren et al. [30] proposed a nonlocal operator method applicable to solving partial differential equations of mechanical problems. Zhuang et al. [31] presented a nonlocal operator method for dynamic fracture exploiting an explicit phase-field model.

Yang et al. [29] introduced the concept of "double-horizon peridynamics" with an intention to reduce computational time of peridynamic simulations. Double-horizon peridynamics is different than the dual-horizon peridynamics developed by Ren et al [30]. Derivation of dual-horizon peridynamics based on Euler-Lagrange formulation is presented in Wang et al [31]. In double-horizon peridynamics, each material point has two horizons, whereas, in dual-horizon peridynamics, each interacting material point has a different horizon and size. More information about peridynamics literature can be found in Javili et al [32].

In this study, the double-horizon peridynamics formulation presented by Yang et al. [29] for one-dimensional structures is extended to two-dimensional structures, especially for a membrane. First, the details of the formulation are given. Next, the treatment of boundary conditions in the double-horizon peridynamics framework is provided. Then, analytical solutions for different boundary conditions are given. Finally, several numerical cases are presented by considering different boundary conditions for static or dynamic problems.

2. Two-dimensional double-horizon peridynamic formulation

2.1. Classical PD formulation

The equation of motion (EOM) for a two-dimensional membrane in classical continuum mechanics (CCM) can be written as:

$$\frac{\partial^2 w}{\partial t^2}(x,y,t) = c^2\left(\frac{\partial^2 w}{\partial x^2}(x,y,t) + \frac{\partial^2 w}{\partial y^2}(x,y,t)\right) + f(x,y,t). \tag{2.1}$$

Taylor expansion can be used to convert the Laplace term into nonlocal form as:

$$w(\boldsymbol{x}+\boldsymbol{\xi}) - w(\boldsymbol{x}) = \left.\frac{\partial w}{\partial x_i}\right|_x \xi n_i + \frac{1}{2}\left.\frac{\partial^2 w}{\partial x_i \partial x_j}\right|_x \xi^2 n_i n_j + \frac{1}{3!}\left.\frac{\partial^3 w}{\partial x_i \partial x_j \partial x_k}\right|_x \xi^3 n_i n_j n_k + O(\xi^4). \tag{2.2}$$

As shown in Figure 1, $\xi = \|\boldsymbol{\xi}\|$ represents the distance between two material points, and n_i represents the component of unit orientation vector such that

$$n_i = \left\{\begin{matrix} n_1 \\ n_2 \end{matrix}\right\} = \left\{\begin{matrix} \cos\varphi \\ \sin\varphi \end{matrix}\right\} \tag{2.3}$$
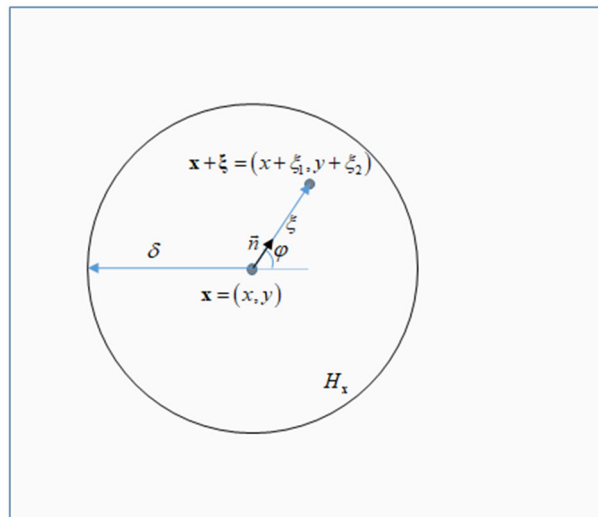
and $O(\xi^4)$ denotes the truncation error.

Figure 1. Peridynamic horizon in classical PD formulation.

Considering $\boldsymbol{x}$ as fixed, multiplying each term of Eq (2.2) by an attenuated kernel function $\frac{1}{\xi}$ and integrating over the PD horizon gives

$$\int_0^{2\pi}\int_0^{\delta}\frac{w(x+\xi)-w(x)}{\xi}\xi d\xi d\varphi = \frac{\partial w}{\partial x_i}\bigg|_x \int_0^{2\pi}\int_0^{\delta} n_i\xi d\xi d\varphi + \frac{1}{2}\frac{\partial^2 w}{\partial x_i \partial x_j}\bigg|_x \int_0^{2\pi}\int_0^{\delta}\xi n_i n_j\xi d\xi d\varphi$$

$$+\frac{1}{3!}\frac{\partial^3 w}{\partial x_i \partial x_j \partial x_k}\bigg|_x \int_0^{2\pi}\int_0^{\delta}\xi^2 n_i n_j n_k \xi d\xi d\varphi + \int_0^{2\pi}\int_0^{\delta}O(\xi^3)\xi d\xi d\varphi \tag{2.4}$$

which implies

$$\frac{\partial^2 w}{\partial x_i \partial x_i} = \frac{6}{\pi\delta^3}\int_0^{2\pi}\int_0^{\delta}\frac{w(x+\xi)-w(x)}{\xi}\xi d\xi d\varphi - O(\delta^4) \tag{2.5}$$

Plugging Eq (2.5) back into (2.1) yields:

$$\frac{\partial^2 w}{\partial t^2}(x,y,t) = c^2\frac{6}{\pi\delta^3}\int_0^{2\pi}\int_0^{\delta}\frac{w(x+\xi_1,y+\xi_2,t)-w(x,y,t)}{\xi}\xi d\xi d\varphi + f(x,y,t) - O(\delta^4) \tag{2.6}$$

Eq (2.6) reduces to the classical PD equation of motion if we neglect the residual term:

$$\frac{\partial^2 w}{\partial t^2}(x,y,t) = \frac{6c^2}{\pi\delta^3}\int_0^{2\pi}\int_0^{\delta}\frac{w(x+\xi_1,y+\xi_2,t)-w(x,y,t)}{\xi}\xi d\xi d\varphi + f(x,y,t) \tag{2.7}$$

2.2. Double-horizon peridynamics

One can observe from Eq (2.5) that there exists a truncation error between the classical Laplace expression and the PD Laplace expression. As a consequence, the PD equation of motion, Eq (2.7), differs from the corresponding CCM, Eq (2.1), on the order of $O(\delta^4)$. One can reduce this error by choosing a small horizon size, δ. However, this will weaken the nonlocal characteristic of PD. On the other hand, with a large horizon size, δ, enhances PD nonlocal characteristics but can have negative effects on solution accuracy. Such contradiction is a common issue in most PD studies and can be overcome by the double-horizon peridynamics formulation. Moreover, double-horizon peridynamics can provide a computational advantage by utilising two horizons for each material point. In the double-horizon peridynamics formulation, a smaller inner horizon is introduced inside the original horizon, as shown in Figure 2. In this section, details of double-horizon peridynamics are presented for two-dimensional membranes.
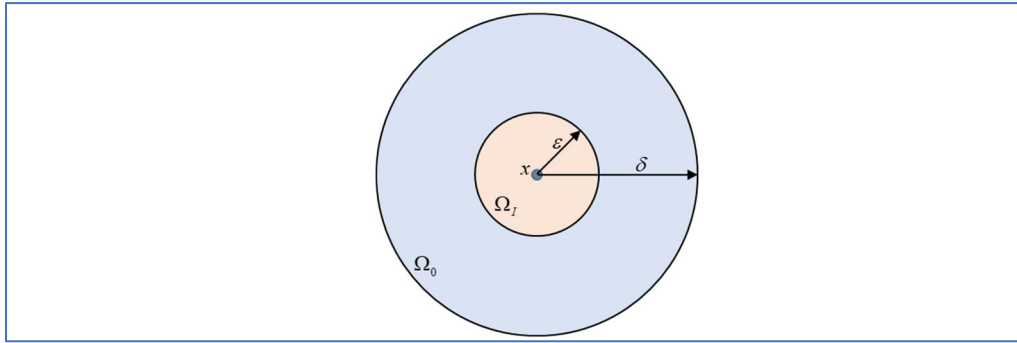
Figure 2. Inner and outer horizons in the double-horizon peridynamics formulation.

First, we know from Eq (2.5) that the nonlocal Laplace term within the inner horizon, Ω_I can be expressed as

$$\frac{\partial^2 w}{\partial x_i \partial x_i} = \frac{6}{\pi \varepsilon^3} \int_0^{2\pi} \int_0^{\varepsilon} \frac{w(\boldsymbol{x} + \boldsymbol{\xi}) - w(\boldsymbol{x})}{\xi} \xi d\xi d\varphi - O(\varepsilon^4) \tag{2.8}$$

Note that the inner horizon size can be chosen as arbitrarily small so that $0 \approx O(\varepsilon^4) \ll O(\delta^4)$ so that the residual is negligible.

Next, let us consider the nonlocal Laplace term over the outer horizon, Ω_O. Multiplying each term in Eq (2.2) by $\frac{1}{\xi}$ gives

$$\frac{w(\boldsymbol{x} + \boldsymbol{\xi}) - w(\boldsymbol{x})}{\xi} = \frac{\partial w}{\partial x_i}\bigg|_{\boldsymbol{x}} n_i + \frac{1}{2} \frac{\partial^2 w}{\partial x_i \partial x_j}\bigg|_{\boldsymbol{x}} \xi n_i n_j + \frac{1}{3!} \frac{\partial^3 w}{\partial x_i \partial x_j \partial x_k}\bigg|_{\boldsymbol{x}} \xi^2 n_i n_j n_k + O(\xi^3) \tag{2.9}$$

Note that when ξ varies over the outer horizon, the truncation error ranges as

$$\left| O(\varepsilon^3) \right| \leq \left| O(\xi^3) \right| \leq \left| O(\delta^3) \right| \tag{2.10}$$

In order to minimize the truncation error so that it levels with that of the inner horizon, we can multiply Eq (2.9) by $\frac{\varepsilon^3}{\xi^3}$:

$$\frac{\varepsilon^3}{\xi^3} \frac{w(\boldsymbol{x} + \boldsymbol{\xi}) - w(\boldsymbol{x})}{\xi} = \frac{\partial w}{\partial x_i}\bigg|_{\boldsymbol{x}} \frac{\varepsilon^3}{\xi^3} n_i + \frac{1}{2} \frac{\partial^2 w}{\partial x_i \partial x_j}\bigg|_{\boldsymbol{x}} \frac{\varepsilon^3}{\xi^2} n_i n_j + \frac{1}{3!} \frac{\partial^3 w}{\partial x_i \partial x_j \partial x_k}\bigg|_{\boldsymbol{x}} \frac{\varepsilon^3}{\xi} n_i n_j n_k + O(\varepsilon^3) \tag{2.11}$$

Integrating Eq (2.11) over the outer horizon gives

$$\int_{\Omega_O} \frac{\varepsilon^3}{\xi^3} \frac{w(x+\xi)-w(x)}{\xi} d\Omega_O = \frac{\partial w}{\partial x_i}\bigg|_x \int_{\Omega_O} \frac{\varepsilon^3}{\xi^3} n_i d\Omega_O + \frac{1}{2}\frac{\partial^2 w}{\partial x_i \partial x_j}\bigg|_x \int_{\Omega_O} \frac{\varepsilon^3}{\xi^2} n_i n_j d\Omega_O$$
$$+ \frac{1}{3!}\frac{\partial^3 w}{\partial x_i \partial x_j \partial x_k}\bigg|_x \int_{\Omega_O} \frac{\varepsilon^3}{\xi} n_i n_j n_k d\Omega_O + \int_{\Omega_O} O(\varepsilon^3) d\Omega_O \qquad (2.12)$$

Ignoring the residual results in the nonlocal Laplace term with respect to outer horizon as

$$\frac{\partial^2 w}{\partial x_i \partial x_i} = \frac{2}{\pi \varepsilon^3 \ln(\delta/\varepsilon)} \int_0^{2\pi} \int_\varepsilon^\delta \frac{\varepsilon^3}{\xi^3} \frac{w(x+\xi)-w(x)}{\xi} \xi d\xi d\varphi \qquad (2.13)$$

Introducing two weight functions ω_I and ω_O for inner and outer horizon, respectively, such that

$$\omega_I + \omega_O = 1 \qquad (2.14)$$

Coupling Eq (2.8) and (2.14) with the introduction of weight functions gives

$$\frac{\partial^2 w}{\partial x_i \partial x_i} = \omega_I \frac{6}{\pi \varepsilon^3} \int_0^{2\pi} \int_0^\varepsilon \frac{w(x+\xi)-w(x)}{\xi} \xi d\xi d\varphi + \omega_O \frac{2}{\pi \varepsilon^3 \ln(\delta/\varepsilon)} \int_0^{2\pi} \int_\varepsilon^\delta \frac{\varepsilon^3}{\xi^3} \frac{w(x+\xi)-w(x)}{\xi} \xi d\xi d\varphi \quad (2.15)$$

in which the weight functions can be chosen by considering each area in proportion to the total horizon area as

$$\omega_I = \frac{\varepsilon^2}{\delta^2} \quad \text{and} \quad \omega_O = \frac{\delta^2 - \varepsilon^2}{\delta^2} \qquad (2.16)$$

Coupling Eq (2.15) with (2.16) and substituting back into (2.1) yields the refined PD equation of motion for membrane structure as

$$\frac{\partial^2 w}{\partial t^2}(x,y,t) = \left\{ \begin{array}{l} k_I \displaystyle\int_0^{2\pi} \int_0^\varepsilon \frac{w(x+\xi_1,y+\xi_2,t)-w(x,y,t)}{\xi} \xi d\xi d\varphi \\[2mm] + k_O \displaystyle\int_0^{2\pi} \int_\varepsilon^\delta \frac{\varepsilon^3}{\xi^3} \frac{w(x+\xi_1,y+\xi_2,t)-w(x,y,t)}{\xi} \xi d\xi d\varphi \end{array} \right\} + f(x,y,t) \qquad (2.17a)$$

In particular, it reduces to static case when eliminating the inertia term:

$$k_I \int_0^{2\pi} \int_0^\varepsilon \frac{w(x+\xi_1,y+\xi_2)-w(x,y)}{\xi} \xi d\xi d\varphi + k_O \int_0^{2\pi} \int_\varepsilon^\delta \frac{\varepsilon^3}{\xi^3} \frac{w(x+\xi_1,y+\xi_2)-w(x,y)}{\xi} \xi d\xi d\varphi + f(x,y) = 0 \quad (2.17b)$$

where

$$k_I = c^2 \frac{\varepsilon^2}{\delta^2} \frac{6}{\pi \varepsilon^3} \quad \text{and} \quad k_O = c^2 \frac{2(\delta^2 - \varepsilon^2)}{\delta^2 \ln(\delta / \varepsilon)} \frac{1}{\pi \varepsilon^3} \tag{2.18}$$

which represent PD parameters with respect to inner and outer horizons, respectively.

Note that when the inner horizon radius is equal to the outer horizon radius, $\varepsilon = \delta$, Eq (2.17a) and (2.17b) reduce to the traditional PD form.

3. Boundary conditions

Eq (2.17) holds if and only if each integration domain is intact. In other words, the total PD horizon of each material point is completely embedded in the body. However, for some material points adjacent to the boundary whose PD horizon is incomplete, we can introduce a fictitious region with a width of δ outside the body to ensure that Eq (2.17) holds for the entire body, as shown in Figure 3. The displacement field of the fictitious region is related to the real body to achieve a different kind of boundary conditions, and two common cases are explained below.
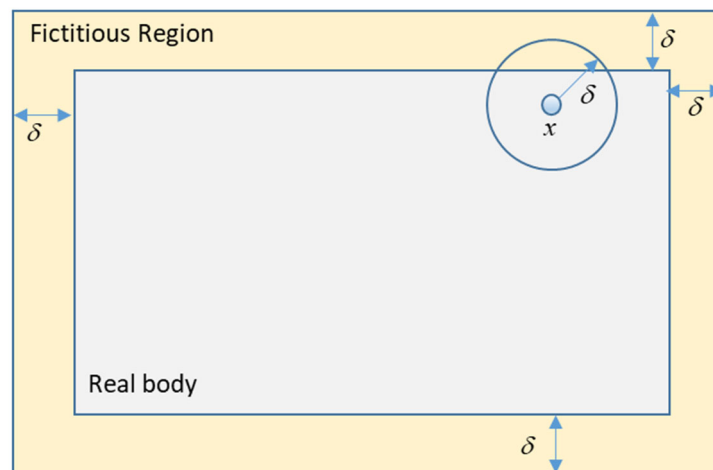

Figure 3. Real and fictitious regions for peridynamic solution domain.

3.1. Clamped edge (C)

Consider a body subjected to a fixed constrain at the edge $x = x^*$. Geometrically, this implies a zero curvature during deformation such that

$$w(x^*, y, t) = 0 \tag{3.1a}$$

$$\left. \frac{\partial^2 w}{\partial x^2} \right|_{(x^*, y, t)} = 0 \tag{3.1b}$$

By performing central difference

$$\frac{w\left(x^* - \xi, y, t\right) - 2w\left(x^*, y, t\right) + w\left(x^* + \xi, y, t\right)}{\xi^2} \tag{3.2}$$

and substituting Eq (3.1a) back into Eq (3.2) yields:

$$w\left(x^* - \xi, y, t\right) = -w\left(x^* + \xi, y, t\right) \quad \forall \xi \in [0, \delta] \tag{3.3a}$$

Similarly, a fixed boundary along the edge $y = y^*$ satisfies the following:

$$w\left(x, y^* - \xi, t\right) = -w\left(x, y^* + \xi, t\right) \quad \forall \xi \in [0, \delta] \tag{3.3b}$$

One can observe that a fixed boundary manipulates an anti-symmetric displacement relationship between real and fictitious regions with respect to the boundary.

3.2. Free edge (F)

Consider a body subjected to free boundary at the edge $x = x^*$ and geometrically, which implies a zero slope about y axis such that

$$\left.\frac{\partial w}{\partial x}\right|_{\left(x^*, y, t\right)} = 0 \tag{3.4}$$

Performing central difference yields

$$\frac{w\left(x^* - \xi, y, t\right) - w\left(x^* + \xi, y, t\right)}{2\xi} = 0 \quad \Rightarrow \quad w\left(x^* - \xi, y, t\right) = w\left(x^* + \xi, y, t\right) \quad \forall \xi \in [0, \delta] \tag{3.5a}$$

Similarly, for free edge along $y = y^*$, the PD boundary condition will be

$$w\left(x^*, y - \xi, t\right) = w\left(x^*, y + \xi, t\right) \quad \forall \xi \in [0, \delta] \tag{3.5b}$$

One can observe that a free boundary manipulates a symmetric displacement relation between real and fictitious regions with respect to the boundary.

4. Analytical solution for static cases

4.1. Rectangular membrane with four fixed edges (CCCC)

Consider a rectangular membrane with four fixed (clamped) edges (CCCC) subjected to some arbitrarily distributed load, as shown in Figure 4.
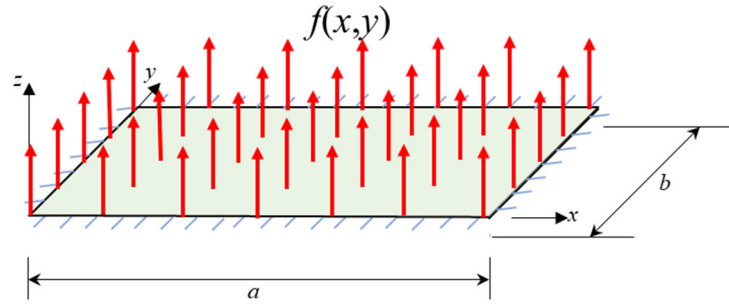
Figure 4. Rectangular membrane with four fixed edges (CCCC).

As explained above, the PD boundary conditions can be given as

$$\begin{cases} w(-\xi,y) = -w(\xi,y) \\ w(a+\xi,y) = -w(a-\xi,y) \\ w(x,-\xi) = -w(x,\xi) \\ w(x,b+\xi) = -w(x,b-\xi) \end{cases} \quad \forall \xi \in [0,\delta] \tag{4.1}$$

If we periodically extend such relationship over the entire xy-plane, one can obtain a periodic displacement field with respect to x-direction and it is skew-symmetric about $(x,y) = (2na,y)$ for any integers n, with period of $2a$. With respect to y-direction, it is skew-symmetric about $(x,y) = (x,2nb)$ for any integers n, with period of $2b$.

Therefore, an admissible function can be chosen as

$$w(x,y) = \sum_{m=1}^{\infty}\sum_{n=1}^{\infty} A_{mn} \sin(\bar{m}x)\sin(\bar{n}y) \tag{4.2}$$

where

$$\bar{m} = \frac{m\pi}{a} \quad \text{and} \quad \bar{n} = \frac{n\pi}{b} \tag{4.3}$$

Substituting Eq (4.25) into Eq (2.17b) yields

$$\sum_{m=1}^{\infty}\sum_{n=1}^{\infty} A_{mn}\left[k_I \int_0^{2\pi}\int_0^{\varepsilon} \frac{1-\cos\bar{m}\xi_1\cos\bar{n}\xi_2}{\xi}\xi d\xi d\varphi + k_O \int_0^{2\pi}\int_\varepsilon^{\delta} \frac{\varepsilon^3}{\xi^3}\frac{1-\cos\bar{m}\xi_1\cos\bar{n}\xi_2}{\xi}\xi d\xi d\varphi \right]\sin\bar{m}x\sin\bar{n}y = f(x,y) \tag{4.4}$$

where the coefficients can be obtained based on orthogonality conditions as

$$A_{mn} = \frac{\dfrac{4}{ab}\displaystyle\int_0^b\int_0^a f(x,y)\sin\bar{m}x\sin\bar{n}y\,dxdy}{k_I \displaystyle\int_0^{2\pi}\int_0^{\varepsilon} \frac{1-\cos\bar{m}\xi_1\cos\bar{n}\xi_2}{\xi}\xi d\xi d\varphi + k_O \displaystyle\int_0^{2\pi}\int_\varepsilon^{\delta} \frac{\varepsilon^3}{\xi^3}\frac{1-\cos\bar{m}\xi_1\cos\bar{n}\xi_2}{\xi}\xi d\xi d\varphi} \tag{4.5}$$

Substituting Eq (4.5) into (4.2) results in the analytical solution to PD double-horizon model as

$$
w(x,y) = \sum_{m=1}^{\infty}\sum_{n=1}^{\infty} \frac{\dfrac{4}{ab}\left[\displaystyle\int_0^b\int_0^a f(x,y)\sin(\overline{m}x)\sin(\overline{n}y)\,dxdy\right]\sin(\overline{m}x)\sin(\overline{n}y)}{k_I\displaystyle\int_0^{2\pi}\int_0^{\varepsilon}\frac{1-\cos(\overline{m}\xi_1)\cos(\overline{n}\xi_2)}{\xi}\xi\,d\xi d\varphi + k_O\displaystyle\int_0^{2\pi}\int_{\varepsilon}^{\delta}\frac{\varepsilon^3}{\xi^3}\frac{1-\cos(\overline{m}\xi_1)\cos(\overline{n}\xi_2)}{\xi}\xi\,d\xi d\varphi}
\tag{4.6}
$$

In particular, when $\varepsilon = \delta$, Eq (4.6) reduces to the solution for the classical PD model:

$$
w(x,y) = \frac{4}{ab}\frac{1}{c^2}\frac{\pi\delta^3}{6}\sum_{m=1}^{\infty}\sum_{n=1}^{\infty}\frac{\left[\displaystyle\int_0^b\int_0^a f(x,y)\sin(\overline{m}x)\sin(\overline{n}y)\,dxdy\right]\sin(\overline{m}x)\sin(\overline{n}y)}{\displaystyle\int_0^{2\pi}\int_0^{\delta}\frac{1-\cos(\overline{m}\xi_1)\cos(\overline{n}\xi_2)}{\xi}\xi\,d\xi d\varphi}
\tag{4.7}
$$

Regarding boundary conditions of CCFF and CCCF, the corresponding solutions can be obtained from Eq (4.6) by letting:

$$
\text{CCFF:}\quad \overline{m} = \frac{(2m-1)\pi}{2a} \quad\text{and}\quad \overline{n} = \frac{(2n-1)\pi}{2b}
\tag{4.8}
$$

$$
\text{CCCF:}\quad \overline{m} = \frac{m\pi}{a} \quad\text{and}\quad \overline{n} = \frac{(2n-1)\pi}{2b}
\tag{4.9}
$$

4.2. Rectangular membrane with mixed boundary conditions (CFCF)

Consider a rectangular membrane with two opposite edges clamped and others free subjected to some arbitrarily distributed load, as shown in Figure 5.
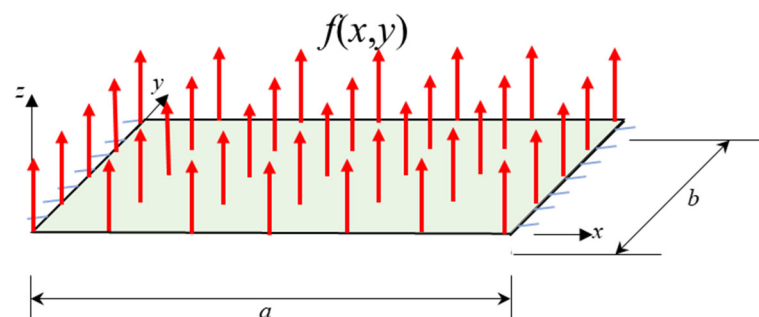

Figure 5. Rectangular membrane with mixed boundary conditions (CFCF).

As explained above, the PD boundary conditions can be written as

$$\begin{cases} w(-\xi, y) = -w(\xi, y) \\ w(a+\xi, y) = -w(a-\xi, y) \\ w(x, -\xi) = w(x, \xi) \\ w(x, b+\xi) = w(x, b-\xi) \end{cases} \quad \forall \xi \in [0, \delta] \tag{4.10}$$

Obeying such relationship and periodically extending the displacement field over the entire xy-plane, one admissible solution can be selected as

$$w(x, y) = \sum_{m=1}^{\infty} \sum_{n=0}^{\infty} A_{mn} \sin(\bar{m}x) \cos(\bar{n}y) \tag{4.11}$$

where

$$\bar{m} = \frac{m\pi}{a} \quad \text{and} \quad \bar{n} = \frac{n\pi}{b} \tag{4.12}$$

Substituting Eq (4.11) back into Eq (2.17b), one can obtain

$$\sum_{m=1}^{\infty} \sum_{n=0}^{\infty} A_{mn} \left[k_I \int_0^{2\pi} \int_0^{\varepsilon} \frac{1 - \cos\bar{m}\xi_1 \cos\bar{n}\xi_2}{\xi} \xi d\xi d\varphi + k_O \int_0^{2\pi} \int_\varepsilon^\delta \frac{\varepsilon^3}{\xi^3} \frac{1 - \cos\bar{m}\xi_1 \cos\bar{n}\xi_2}{\xi} \xi d\xi d\varphi \right] \sin\bar{m}x \cos\bar{n}y = f(x, y) \tag{4.13}$$

where the coefficients can be obtained as

$$\begin{cases} A_{mn} = \dfrac{\dfrac{4}{ab} \displaystyle\int_0^b \int_0^a f(x, y) \sin(\bar{m}x) \cos(\bar{n}y) dx dy}{k_I \displaystyle\int_0^{2\pi} \int_0^{\varepsilon} \frac{1}{\xi} \left(1 - \cos\bar{m}\xi_1 \cos\bar{n}\xi_2\right) \xi d\xi d\varphi + k_O \displaystyle\int_0^{2\pi} \int_\varepsilon^\delta \frac{\varepsilon^3}{\xi^3} \frac{1}{\xi} \left(1 - \cos\bar{m}\xi_1 \cos\bar{n}\xi_2\right) \xi d\xi d\varphi} \quad m, n \geq 1 \\[2em] A_{m0} = \dfrac{\dfrac{2}{ab} \displaystyle\int_0^b \int_0^a f(x, y) \sin(\bar{m}x) dx dy}{k_I \displaystyle\int_0^{2\pi} \int_0^{\varepsilon} \frac{1}{\xi} \left(1 - \cos\bar{m}\xi_1\right) \xi d\xi d\varphi + k_O \displaystyle\int_0^{2\pi} \int_\varepsilon^\delta \frac{\varepsilon^3}{\xi^3} \frac{1}{\xi} \left(1 - \cos\bar{m}\xi_1\right) \xi d\xi d\varphi} \quad m \geq 1, n = 0 \end{cases} \tag{4.14}$$

Substituting Eq (4.14) in Eq (4.11) yields

$$w(x, y) = \sum_{m=1}^{\infty} \left\{ \frac{\dfrac{2}{ab} \displaystyle\int_0^b \int_0^a f(x, y) \sin(\bar{m}x) dx dy}{k_I \displaystyle\int_0^{2\pi} \int_0^{\varepsilon} \frac{1}{\xi}\left(1 - \cos\bar{m}\xi_1\right) \xi d\xi d\varphi + k_O \displaystyle\int_0^{2\pi} \int_\varepsilon^\delta \frac{\varepsilon^3}{\xi^3} \frac{1}{\xi}\left(1 - \cos\bar{m}\xi_1\right) \xi d\xi d\varphi} + \sum_{n=1}^{\infty} \left[\frac{\dfrac{4}{ab} \displaystyle\int_0^b \int_0^a f(x, y) \sin(\bar{m}x) \cos(\bar{n}y) dx dy}{k_I \displaystyle\int_0^{2\pi} \int_0^{\varepsilon} \frac{1 - \cos\bar{m}\xi_1 \cos\bar{n}\xi_2}{\xi} \xi d\xi d\varphi + k_O \displaystyle\int_0^{2\pi} \int_\varepsilon^\delta \frac{\varepsilon^3}{\xi^3} \frac{1 - \cos\bar{m}\xi_1 \cos\bar{n}\xi_2}{\xi} \xi d\xi d\varphi} \right] \cos\bar{n}y \right\} \sin\bar{m}x \tag{4.15}$$

Again, letting $\varepsilon = \delta$ reduces to the solution for the classical PD model as

$$w(x,y) = \frac{4}{ab}\frac{1}{c^2}\frac{\pi\delta^3}{6}\sum_{m=1}^{\infty}\left\{\frac{\frac{1}{2}\int_0^b\int_0^a f(x,y)\sin\bar{m}x\,dxdy}{\int_0^{2\pi}\int_0^\delta\frac{1-\cos\bar{m}\xi_1}{\xi}\xi d\xi d\varphi}+\sum_{n=1}^{\infty}\frac{\int_0^b\int_0^a f(x,y)\sin\bar{m}x\cos\bar{n}y\,dxdy}{\int_0^{2\pi}\int_0^\varepsilon\frac{1-\cos\bar{m}\xi_1\cos\bar{n}\xi_2}{\xi}\xi d\xi d\varphi}\cos\bar{n}y\right\}\sin\bar{m}x \quad (4.16)$$

Regarding boundary conditions of CFFF, the corresponding solution can be obtained from Eq (4.15) by letting:

$$\bar{m} = \frac{(2m-1)\pi}{2a} \quad \text{and} \quad \bar{n} = \frac{n\pi}{b} \tag{4.17}$$

5. Free vibration

Consider an $a \times b$ rectangular membrane with four edges being clamped. The equation of motion and initial conditions are given as

$$\frac{\partial^2 w}{\partial t^2}(x,y,t) = k_I\int_0^{2\pi}\int_0^\varepsilon\frac{w(x+\xi_1,y+\xi_2,t)-w(x,y,t)}{\xi}\xi d\xi d\varphi + k_O\int_0^{2\pi}\int_\varepsilon^\delta\frac{\varepsilon^3}{\xi^3}\frac{w(x+\xi_1,y+\xi_2,t)-w(x,y,t)}{\xi}\xi d\xi d\varphi \tag{5.1}$$

$$w(x,y,0) = w_0(x,y) \quad \text{and} \quad \frac{\partial w}{\partial t}(x,y,0) = v_0(x,y) \tag{5.2}$$

Let us separate the variables as

$$w(x,y,t) = W(x,y)T(t) \tag{5.3}$$

and substituting back into Eq (5.1):

$$W(x,y)\frac{d^2T(t)}{dt^2} = T(t)\left\{k_I\int_0^{2\pi}\int_0^\varepsilon\frac{W(x+\xi_1,y+\xi_2)-W(x,y)}{\xi}\xi d\xi d\varphi + k_O\int_0^{2\pi}\int_\varepsilon^\delta\frac{\varepsilon^3}{\xi^3}\frac{W(x+\xi_1,y+\xi_2)-W(x,y)}{\xi}\xi d\xi d\varphi\right\} \tag{5.4}$$

which yields

$$\frac{1}{T(t)}\frac{d^2T(t)}{dt^2} = \frac{1}{W(x,y)}\left\{k_I\int_0^{2\pi}\int_0^\varepsilon\frac{W(x+\xi_1,y+\xi_2)-W(x,y)}{\xi}\xi d\xi d\varphi + k_O\int_0^{2\pi}\int_\varepsilon^\delta\frac{\varepsilon^3}{\xi^3}\frac{W(x+\xi_1,y+\xi_2)-W(x,y)}{\xi}\xi d\xi d\varphi\right\} = -\lambda \tag{5.5}$$

where $\lambda \in \mathbb{R}$ is a constant independent of x, y and t. Two characteristic functions can be written as

$$\frac{d^2T(t)}{dt^2} = -\lambda T(t) \tag{5.6a}$$

and

$$k_I\int_0^{2\pi}\int_0^\varepsilon\frac{W(x+\xi_1,y+\xi_2)-W(x,y)}{\xi}\xi d\xi d\varphi + k_O\int_0^{2\pi}\int_\varepsilon^\delta\frac{\varepsilon^3}{\xi^3}\frac{W(x+\xi_1,y+\xi_2)-W(x,y)}{\xi}\xi d\xi d\varphi = -\lambda W(x,y) \tag{5.6b}$$

5.1. Rectangular membrane with four fixed edges (CCCC)

Comparing Eqs (5.6b) with (2.17b), if we consider $W(x,y)$ as an analogue to $w(x,y)$ and $\lambda w(x,y)$ as an analogue to $f(x,y)$, the following can be obtained by utilising Eqs (4.2) and (4.5) as

$$\sum_{m=1}^{\infty}\sum_{n=1}^{\infty}A_{mn}\left\{k_I\int_0^{2\pi}\int_0^{\varepsilon}\frac{1-\cos(\bar{m}\xi_1)\cos(\bar{n}\xi_2)}{\xi}\xi d\xi d\varphi+k_O\int_0^{2\pi}\int_\varepsilon^{\delta}\frac{\varepsilon^3}{\xi^3}\frac{1-\cos(\bar{m}\xi_1)\cos(\bar{n}\xi_2)}{\xi}\xi d\xi d\varphi\right\}\sin(\bar{m}x)\sin(\bar{n}y)$$
$$=\sum_{m=1}^{\infty}\sum_{n=1}^{\infty}\lambda A_{mn}\sin(\bar{m}x)\sin(\bar{n}y) \tag{5.7}$$

By comparing corresponding coefficients on both sides, the eigenvalues can be obtained as

$$\lambda_{mn}=k_I\int_0^{2\pi}\int_0^{\varepsilon}\frac{1-\cos(\bar{m}\xi_1)\cos(\bar{n}\xi_2)}{\xi}\xi d\xi d\varphi+k_O\int_0^{2\pi}\int_\varepsilon^{\delta}\frac{\varepsilon^3}{\xi^4}\frac{1-\cos(\bar{m}\xi_1)\cos(\bar{n}\xi_2)}{\xi}\xi d\xi d\varphi \tag{5.8}$$

The general solution to Eq (5.6a) can be written as

$$T_{mn}(t)=A_{mn}\cos\left(\sqrt{\lambda_{mn}}t\right)+B_{mn}\sin\left(\sqrt{\lambda_{mn}}t\right) \tag{5.9}$$

According to the superposition principle, the general solution to Eq (5.3) can be written as a linear combination of each mode as

$$w(x,y,t)=\sum_{m=1}^{\infty}\sum_{n=1}^{\infty}\left[A_{mn}\cos\left(\sqrt{\lambda_{mn}}t\right)+B_{mn}\sin\left(\sqrt{\lambda_{mn}}t\right)\right]\sin(\bar{m}x)\sin(\bar{n}y) \tag{5.10}$$

and initial conditions can be written as

$$w_0(x,y)=\sum_{m=1}^{\infty}\sum_{n=1}^{\infty}A_{mn}\sin(\bar{m}x)\sin(\bar{n}y) \tag{5.11a}$$

$$v_0(x,y)=\sum_{m=1}^{\infty}\sum_{n=1}^{\infty}B_{mn}\sqrt{\lambda_{mn}}\sin(\bar{m}x)\sin(\bar{n}y) \tag{5.11b}$$

where the coefficients can be obtained as

$$A_{mn}=\frac{4}{ab}\int_0^b\int_0^a w_0(x,y)\sin(\bar{m}x)\sin(\bar{n}y)dxdy \tag{5.12a}$$

$$B_{mn}=\frac{4}{ab}\frac{1}{\sqrt{\lambda_{mn}}}\int_0^b\int_0^a v_0(x,y)\sin(\bar{m}x)\sin(\bar{n}y)dxdy \tag{5.12b}$$

In summary, the complete solution for CCCC is:

$$w(x,y,t) = \sum_{m=1}^{\infty}\sum_{n=1}^{\infty}\left[A_{mn}\cos\left(\sqrt{\lambda_{mn}}\,t\right) + B_{mn}\sin\left(\sqrt{\lambda_{mn}}\,t\right)\right]\sin\left(\bar{m}x\right)\sin\left(\bar{n}y\right)$$

$$A_{mn} = \frac{4}{ab}\int_{0}^{b}\int_{0}^{a}w_0\left(x,y\right)\sin\left(\bar{m}x\right)\sin\left(\bar{n}y\right)dxdy$$

$$B_{mn} = \frac{4}{ab}\frac{1}{\sqrt{\lambda_{mn}}}\int_{0}^{b}\int_{0}^{a}v_0\left(x,y\right)\sin\left(\bar{m}x\right)\sin\left(\bar{n}y\right)dxdy \tag{5.13}$$

$$\lambda_{mn} = k_I\int_{0}^{2\pi}\int_{0}^{\varepsilon}\frac{1-\cos\left(\bar{m}\xi_1\right)\cos\left(\bar{n}\xi_2\right)}{\xi}\xi d\xi d\varphi + k_O\int_{0}^{2\pi}\int_{\varepsilon}^{\delta}\frac{\varepsilon^3}{\xi^4}\frac{1-\cos\left(\bar{m}\xi_1\right)\cos\left(\bar{n}\xi_2\right)}{\xi}\xi d\xi d\varphi$$

$$\xi_1 = \xi\cos\varphi \quad \xi_2 = \xi\sin\varphi \quad \bar{m} = \frac{m\pi}{a} \quad \bar{n} = \frac{n\pi}{b} \quad k_I = c^2\frac{\varepsilon^2}{\delta^2}\frac{6}{\pi\varepsilon^3} \quad k_O = c^2\frac{2\left(\delta^2 - \varepsilon^2\right)}{\delta^2\ln\left(\delta/\varepsilon\right)}\frac{1}{\pi\varepsilon^3}$$

In particular, by setting $\varepsilon = \delta$, Eq (5.13) reduces to the solution of the classical PD model. Regarding boundary conditions of CCFF and CCCF, the corresponding solutions can be obtained from Eq (5.13) by letting:

$$\text{CCFF:}\quad \bar{m} = \frac{(2m-1)\pi}{2a}\quad\text{and}\quad \bar{n} = \frac{(2n-1)\pi}{2b} \tag{5.14a}$$

$$\text{CCCF:}\quad \bar{m} = \frac{m\pi}{a}\quad\text{and}\quad \bar{n} = \frac{(2n-1)\pi}{2b} \tag{5.14b}$$

5.2. Rectangular membrane with mixed boundary conditions (CFCF)

Comparing Eq (5.6b) with (2.17b), if we consider $W(x,y)$ as an analogue to $w(x,y)$ and $\lambda w(x,y)$ as an analogue to $f(x,y)$, the following can be obtained by utilising Eqs (4.11) and (4.13) as

$$\sum_{m=1}^{\infty}\sum_{n=0}^{\infty}A_{mn}\left\{k_I\int_{0}^{2\pi}\int_{0}^{\varepsilon}\frac{1-\cos\bar{m}\xi_1\cos\bar{n}\xi_2}{\xi}\xi d\xi d\varphi + k_O\int_{0}^{2\pi}\int_{\varepsilon}^{\delta}\frac{\varepsilon^3}{\xi^3}\frac{1-\cos\bar{m}\xi_1\cos\bar{n}\xi_2}{\xi}\xi d\xi d\varphi\right\}\sin\bar{m}x\cos\bar{n}y$$
$$= \sum_{m=1}^{\infty}\sum_{n=0}^{\infty}\lambda A_{mn}\sin\bar{m}x\cos\bar{n}y \tag{5.15}$$

By comparing corresponding coefficients on both sides, the eigenvalues can be obtained as

$$\lambda_{mn} = k_I\int_{0}^{2\pi}\int_{0}^{\varepsilon}\frac{1-\cos\left(\bar{m}\xi_1\right)\cos\left(\bar{n}\xi_2\right)}{\xi}\xi d\xi d\varphi + k_O\int_{0}^{2\pi}\int_{\varepsilon}^{\delta}\frac{\varepsilon^3}{\xi^3}\frac{1-\cos\left(\bar{m}\xi_1\right)\cos\left(\bar{n}\xi_2\right)}{\xi}\xi d\xi d\varphi \tag{5.16}$$

The general solution to Eq (5.6a) is:

$$T_{mn}\left(t\right) = A_{mn}\cos\left(\sqrt{\lambda_{mn}}\,t\right) + B_{mn}\sin\left(\sqrt{\lambda_{mn}}\,t\right) \tag{5.17}$$

According to the superposition principle, the general solution to Eq (5.3) can be written as a linear combination of each mode:

$$w(x,y,t) = \sum_{m=1}^{\infty}\sum_{n=0}^{\infty}\left[A_{mn}\cos\left(\sqrt{\lambda_{mn}}\,t\right) + B_{mn}\sin\left(\sqrt{\lambda_{mn}}\,t\right)\right]\sin\overline{m}x\cos\overline{n}y \tag{5.18}$$

and initial conditions can be written as

$$w_0(x,y) = \sum_{m=1}^{\infty}\sum_{n=0}^{\infty}A_{mn}\sin\overline{m}x\cos\overline{n}y \tag{5.19a}$$

$$v_0(x,y) = \sum_{m=1}^{\infty}\sum_{n=0}^{\infty}B_{mn}\sqrt{\lambda_{mn}}\sin\overline{m}x\cos\overline{n}y \tag{5.19b}$$

According to orthogonality, one can obtain:

$$
\begin{aligned}
A_{mn} &= \frac{4}{ab}\int_0^b\int_0^a w_0(x,y)\sin\overline{m}x\cos\overline{n}y\,dxdy & m,n\geq 1 \\[2mm]
A_{m0} &= \frac{2}{ab}\int_0^b\int_0^a w_0(x,y)\sin\overline{m}x\,dxdy & m\geq 1, n=0 \\[2mm]
B_{mn} &= \frac{4}{ab}\frac{1}{\sqrt{\lambda_{mn}}}\int_0^b\int_0^a v_0(x,y)\sin\overline{m}x\cos\overline{n}y\,dxdy & m,n\geq 1 \\[2mm]
B_{m0} &= \frac{2}{ab}\frac{1}{\sqrt{\lambda_{mn}}}\int_0^b\int_0^a v_0(x,y)\sin\overline{m}x\,dxdy & m\geq 1, n=0
\end{aligned}
\tag{5.20}
$$

In summary, the complete solution for CFCF is:

$$
\begin{aligned}
& w(x,y,t) = \sum_{m=1}^{\infty}\sum_{n=0}^{\infty}\left[A_{mn}\cos\left(\sqrt{\lambda_{mn}}\,t\right) + B_{mn}\sin\left(\sqrt{\lambda_{mn}}\,t\right)\right]\sin\overline{m}x\cos\overline{n}y \\[2mm]
& A_{mn} = \frac{4}{ab}\int_0^b\int_0^a w_0(x,y)\sin\overline{m}x\cos\overline{n}y\,dxdy \qquad m,n\geq 1 \\[2mm]
& A_{m0} = \frac{2}{ab}\int_0^b\int_0^a w_0(x,y)\sin\overline{m}x\,dxdy \qquad m\geq 1, n=0 \\[2mm]
& B_{mn} = \frac{4}{ab}\frac{1}{\sqrt{\lambda_{mn}}}\int_0^b\int_0^a v_0(x,y)\sin\overline{m}x\cos\overline{n}y\,dxdy \quad m,n\geq 1 \\[2mm]
& B_{m0} = \frac{2}{ab}\frac{1}{\sqrt{\lambda_{mn}}}\int_0^b\int_0^a v_0(x,y)\sin\overline{m}x\,dxdy \qquad m\geq 1, n=0 \\[2mm]
& \lambda_{mn} = k_I\int_0^{2\pi}\int_0^{\varepsilon}\frac{1-\cos(\overline{m}\xi_1)\cos(\overline{n}\xi_2)}{\xi}\xi d\xi d\varphi + k_O\int_0^{2\pi}\int_{\varepsilon}^{\delta}\frac{\varepsilon^3}{\xi^3}\frac{1-\cos(\overline{m}\xi_1)\cos(\overline{n}\xi_2)}{\xi}\xi d\xi d\varphi \\[2mm]
& \xi_1 = \xi\cos\varphi \quad \xi_2 = \xi\sin\varphi \quad \overline{m} = \frac{m\pi}{a} \quad \overline{n} = \frac{n\pi}{b} \quad k_I = c^2\frac{\varepsilon^2}{\delta^2}\frac{6}{\pi\varepsilon^3} \quad k_O = c^2\frac{2(\delta^2-\varepsilon^2)}{\delta^2\ln(\delta/\varepsilon)}\frac{1}{\pi\varepsilon^3}
\end{aligned}
\tag{5.21}
$$

6. Numerical cases

In order to validate the capability of the current formulation, several numerical cases are considered and compared against the corresponding classical solutions. The numerical solution of equations of peridynamics is usually done by using the meshless approach [36]. Lopez and Pellegrino [37] implemented a spectral method for the space discretization based on the Fourier expansion of the solution while considering the Newmark-β method for the time marching. Jafarzadeh et al. [38] introduced an efficient boundary-adapted spectral method for peridynamic transient diffusion problems with arbitrary boundary conditions. Without loss of generality, membrane dimensions $a \times b = 1\ m \times 1\ m$ and parameter $c = 1\ Nm/kg$ are chosen throughout this section. The outer horizon size of $\delta = 0.1m$ and varying inner horizon sizes of $\varepsilon = \frac{\delta}{50}, \frac{\delta}{10}, \frac{\delta}{5}$ and $\varepsilon = \delta$ (i.e., classical PD model) are considered.

6.1. Static condition

6.1.1. Rectangular membrane with four fixed edges (CCCC)

In this first numerical case, a rectangular plate with four fixed edges (CCCC) subjected to a loading of $f(x, y) = -0.05 \sin\frac{\pi x}{a} \sin\frac{\pi y}{b}$ is considered under static conditions. The deflection of the plate along the central x-axis for different inner horizon values is given in Figure 6a. As shown in Figure 6b, as the inner horizon size decreases, the peridynamic solution approaches the classical solution.
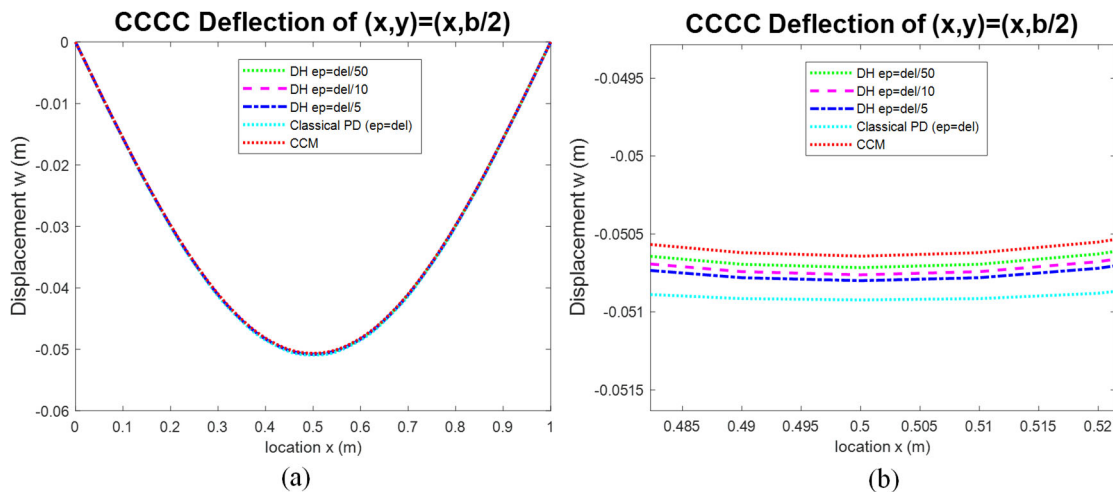

Figure 6. (a) Comparison of PD deflection results with CCM results along x-axis; (b) zoomed view.

6.1.2. Rectangular membrane with mixed boundary conditions (CFCF)

In the second numerical case, for the same loading condition $f(x, y) = -0.05 \sin\frac{\pi x}{a} \sin\frac{\pi y}{b}$, the

rectangular plate is subjected to mixed boundary conditions (CFCF). Deflection values along the central x- and y-axes are given in Figure 7a,c. As in the previous case, the peridynamic solution converges to a classical solution as the inner horizon size decreases (see Figures 7b,d).
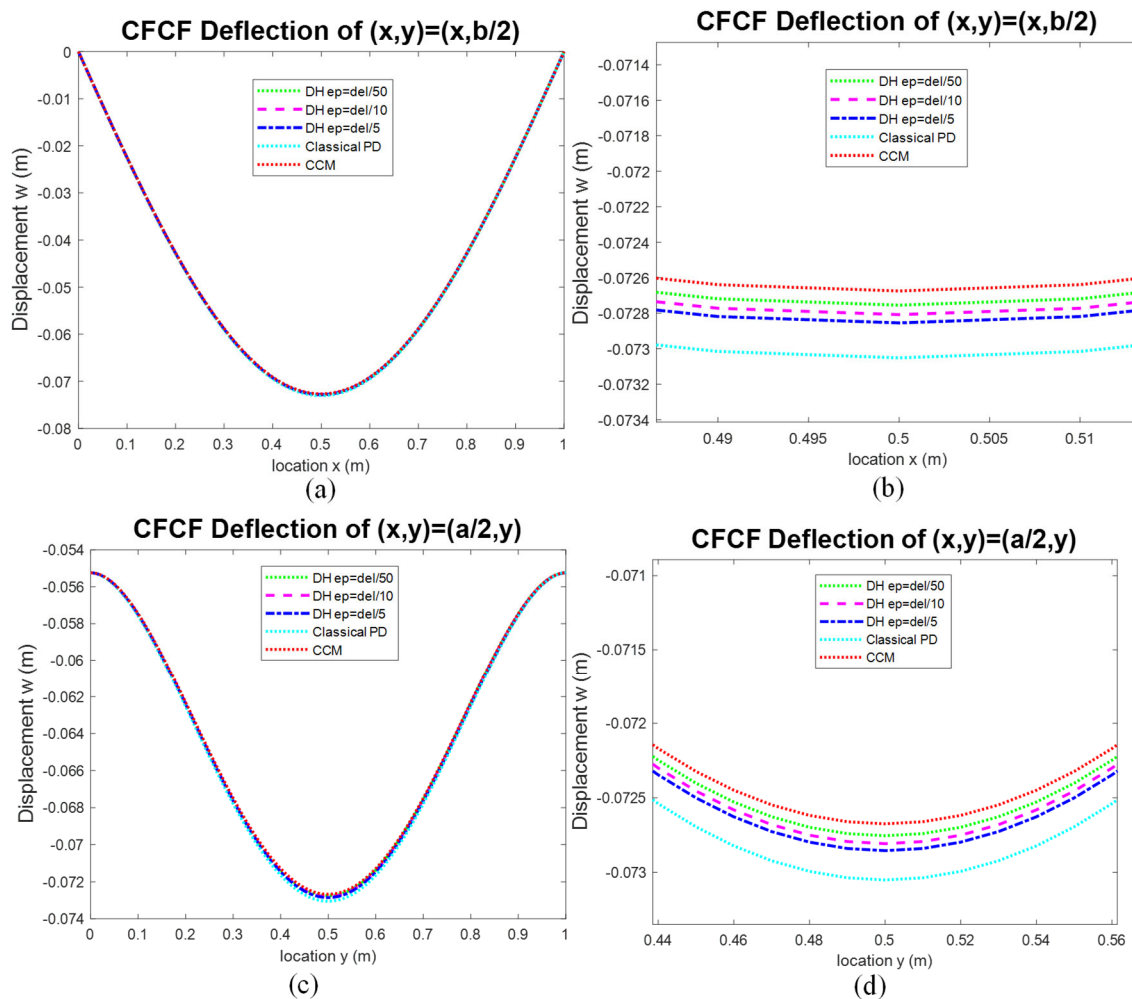

Figure 7. (a) Comparison of PD deflection results with CCM results along x-axis; (b) zoomed view; (c) comparison of PD deflection results with CCM results along y-axis; (d) zoomed view.

6.2. Free vibration condition

6.2.1. Rectangular membrane with four fixed edges (CCCC)

For the next numerical case, the dynamic behavior of the rectangular plate is investigated. The plate has fixed boundaries and is subjected to initial displacement and velocity conditions:

$$\text{ICs:} \quad u_0(x,y) = 0.05x(x-a)y(y-b) \quad v_0(x,y) = \sin\frac{\pi x}{a}\sin\frac{\pi y}{b}$$

Figure 8a demonstrates the variation of the deflection at the center of the rectangular plate as time

progresses. Similar to the static cases, the peridynamic solution converges to the classical solution as the inner horizon size decreases as shown in Figure 8b.
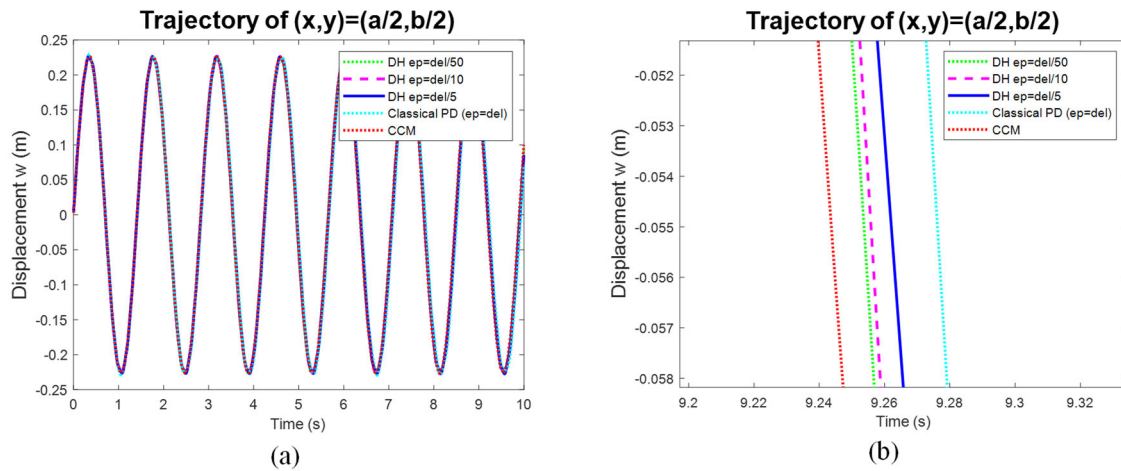

Figure 8. (a) Comparison of PD deflection results with CCM results at the center of the rectangular plate as time progresses; (b) zoomed view.

6.2.2. Rectangular membrane with mixed boundary conditions (CFCF)

For the second dynamic case, the rectangular plate is subjected to the same initial displacement and velocity conditions:

$$\text{ICs:} \quad u_0(x,y) = 0.05x(x-a) \quad v_0(x,y) = -\sin\frac{\pi x}{a}\sin\frac{\pi y}{b}$$

but the edges are subjected to mixed boundary conditions (CFCF). For this boundary condition, the variation of deflection at the center of the plate as time progresses is given in Figure 9a. As shown in Figure 9b, peridynamic and classical solutions become closer as the inner horizon size decreases.
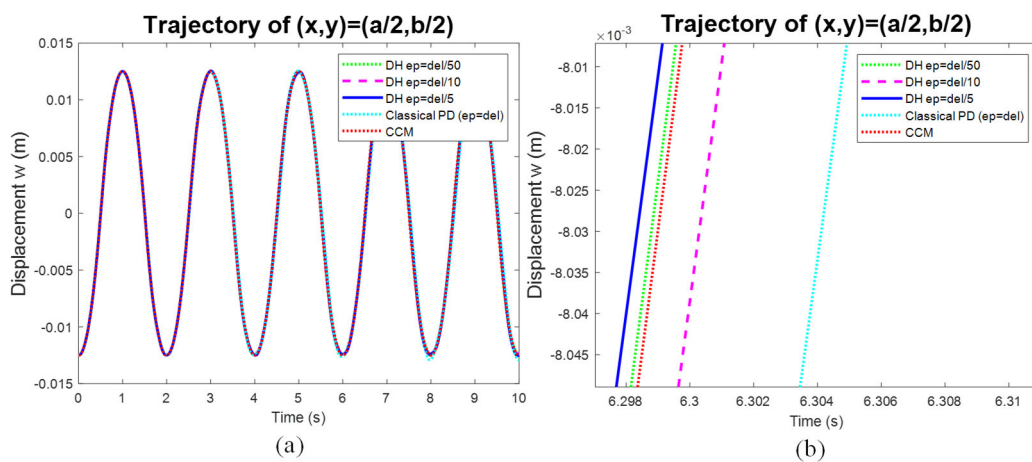

Figure 9. (a) Comparison of PD deflection results with CCM results at the center of the rectangular plate as the time progresses; (b) zoomed view.
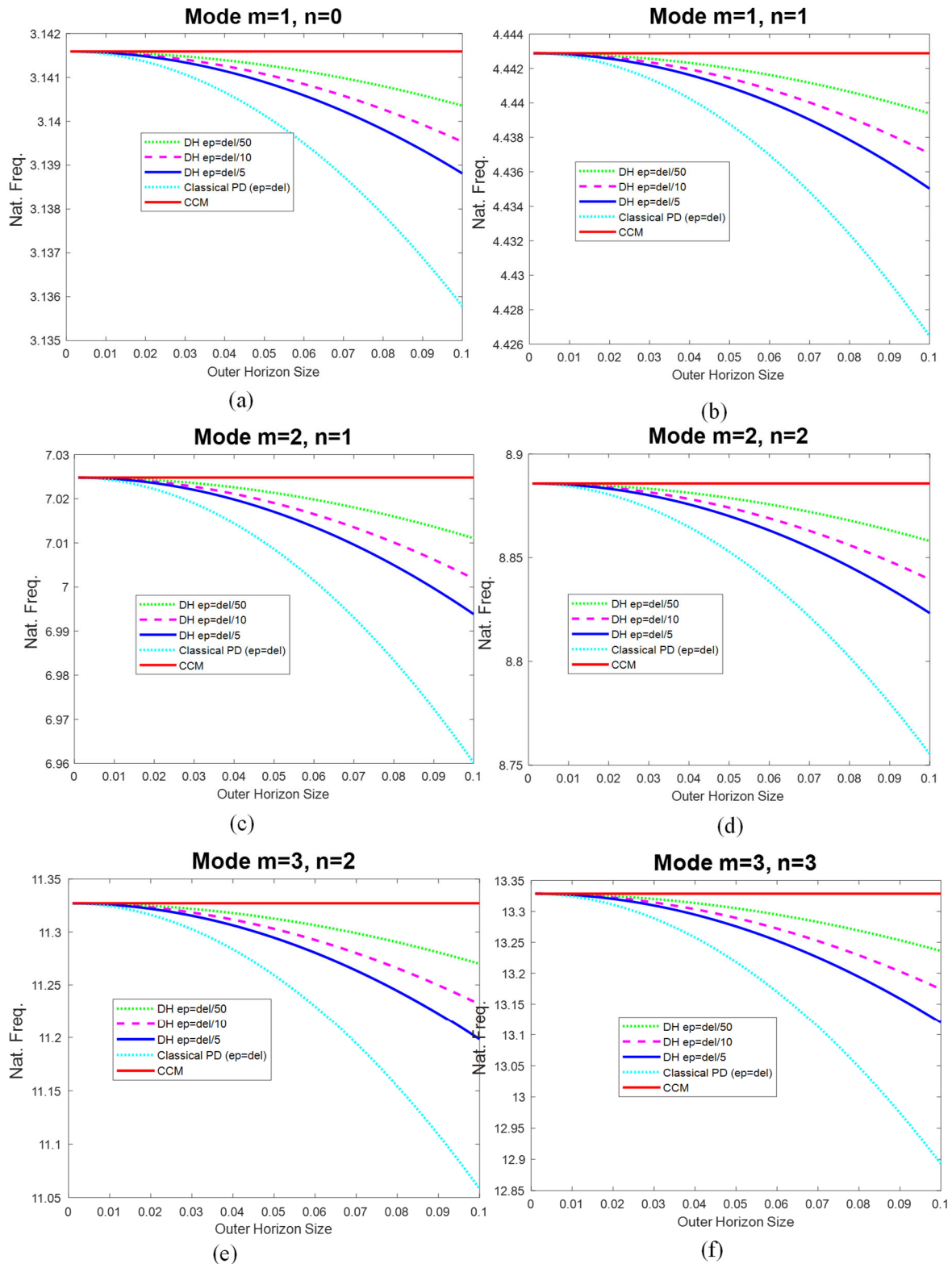
Figure 10. Comparison of PD deflection results with CCM results as the outer horizon size increases. (a) Mode m = 1, n = 0; (b) mode m = 1, n = 1; (c) mode m = 2, n = 1; (d) mode m = 2, n = 2; (e) mode m = 3, n = 2; (f) mode m = 3, n = 3.

6.3. Natural frequencies

For the final numerical case, for the mixed boundary condition (CFCF) for the rectangular membrane, vibrational frequencies of the first 6 modes are compared in Figures 10a–f. According to these figures, it can be seen that as the outer horizon decreases, peridynamic solutions converge to classical solutions and, after certain outer horizon values, these two solutions start diverging due to nonlocal effects. On the other hand, a decreasing inner horizon size can allow representation of the classical behaviour although the outer horizon size is relatively large.

7. Conclusions

In the study, a newly proposed double-horizon peridynamics formulation was presented for two-dimensional membranes subjected to fixed or mixed boundary conditions. Both analytical and numerical solutions are presented. According to the numerical results, it was shown that as the inner horizon size decreases, peridynamic solutions converge to a classical solution for different boundary conditions and both static and dynamic problems. Moreover, it was also demonstrated that for relatively large outer horizon sizes, the inner horizon can allow capturing classical behavior as the inner horizon size decreases. Therefore, it can be concluded that double-horizon peridynamics can provide an alternative platform to reduce computational time by allowing larger horizon sizes but still capturing classical behavior by reducing the inner horizon sizes.

Author contributions

Zhenghao Yang: Conceptualization, Methodology, Formal Analysis, Software, Validation, Visualization, Writing-Original Draft Preparation, Erkan Oterkus: Conceptualization, Methodology, Writing-Review & Editing, Selda Oterkus: Conceptualization, Methodology, Writing-Review & Editing.

Use of AI tools declaration

The authors declare that they have not used Artificial Intelligence (AI) tools in the creation of this article.

Conflict of interest

The authors declare that there is no conflict of interest.

References

1. S. A. Silling, Reformulation of elasticity theory for discontinuities and long-range forces, *J Mech Phys Solids*, **48** (2000), 175–209. https://doi.org/10.1016/S0022-5096(99)00029-0

2. D. De Meo, L. Russo, E. Oterkus, Modeling of the onset, propagation, and interaction of multiple cracks generated from corrosion pits by using peridynamics, *J Eng Mater Techn*, **139** (2017), 041001. https://doi.org/10.1115/1.4036443

3. B. B. Yin, W. K. Sun, Y. Zhang, K. M. Liew, Modeling via peridynamics for large deformation and progressive fracture of hyperelastic materials, *Comput. Methods Appl. Mech. Eng.*, **403** (2023), 115739. https://doi.org/10.1016/j.cma.2022.115739

4. X. Liu, X. He, J. Wang, L. Sun, E. Oterkus, An ordinary state-based peridynamic model for the fracture of zigzag graphene sheets, *Proc. Math. Phys. Eng. Sci.*, **474** (2018), 20180019. https://doi.org/10.1098/rspa.2018.0019

5. M. Dorduncu, Stress analysis of sandwich plates with functionally graded cores using peridynamic differential operator and refined zigzag theory, *Thin Wall Struct*, **146** (2020), 106468. https://doi.org/10.1016/j.tws.2019.106468

6. A. Kutlu, M. Dorduncu, T. Rabczuk, A novel mixed finite element formulation based on the refined zigzag theory for the stress analysis of laminated composite plates, *Compos Struct*, **267** (2021), 113886. https://doi.org/10.1016/j.compstruct.2021.113886

7. W. Chen, X. Gu, Q. Zhang, X. Xia, A refined thermo-mechanical fully coupled peridynamics with application to concrete cracking, *Eng. Fract. Mech.*, **242** (2021), 107463. https://doi.org/10.1016/j.engfracmech.2020.107463

8. M. Qin, D. Yang, W. Chen, S. Yang, Hydraulic fracturing model of a layered rock mass based on peridynamics, *Eng. Fract. Mech.*, **258** (2021), 108088. https://doi.org/10.1016/j.engfracmech.2021.108088

9. A. Lakshmanan, J. Luo, I. Javaheri, V. Sundararaghavan, Three-dimensional crystal plasticity simulations using peridynamics theory and experimental comparison, *Int J Plasticity*, **142** (2021), 102991. https://doi.org/10.1016/j.ijplas.2021.102991

10. H. Yan, M. Sedighi, A. P. Jivkov, Peridynamics modelling of coupled water flow and chemical transport in unsaturated porous media, *J Hydrol*, **591** (2020), 125648. https://doi.org/10.1016/j.jhydrol.2020.125648

11. H. Wang, S. Tanaka, S. Oterkus, E. Oterkus, Study on two-dimensional mixed-mode fatigue crack growth employing ordinary state-based peridynamics, *Theor. Appl. Fract. Mech.*, **124** (2023), 103761. https://doi.org/10.1016/j.tafmec.2023.103761

12. Z. Yang, S. Oterkus, E. Oterkus, Peridynamic formulation for Timoshenko beam, *Procedia Struct. Integr*, **28** (2020), 464–471. https://doi.org/10.1016/j.prostr.2020.10.055

13. Z. Yang, E. Oterkus, S. Oterkus, Peridynamic higher-order beam formulation, *J Peridyn Nonlocal Model*, **3** (2021), 67–83. https://doi.org/10.1007/s42102-020-00043-w

14. Z. Yang, B. Vazic, C. Diyaroglu, E. Oterkus, S. Oterkus, A Kirchhoff plate formulation in a state-based peridynamic framework, *Math Mech Solids*, **25** (2020), 727–738. https://doi.org/10.1177/1081286519887523

15. Z. Yang, E. Oterkus, S. Oterkus, Peridynamic formulation for higher-order plate theory, *J Peridyn Nonlocal Model*, **3** (2021), 185–210. https://doi.org/10.1007/s42102–020–00047–6

16. J. Heo, Z. Yang, W. Xia, S. Oterkus, E. Oterkus, Free vibration analysis of cracked plates using peridynamics, *Ships Offshore Struct*, **15** (2020), S220–S229. https://doi.org/10.1080/17445302.2020.1834266

17. J. Heo, Z. Yang, W. Xia, S. Oterkus, E. Oterkus, Buckling analysis of cracked plates using peridynamics, *Ocean Eng.*, **214** (2020), 107817. https://doi.org/10.1016/j.oceaneng.2020.107817

18. Z. Yang, C. C. Ma, E. Oterkus, S. Oterkus, K. Naumenko, Analytical solution of 1–dimensional peridynamic equation of motion, *J Peridyn Nonlocal Model*, **5** (2023), 356–374. https://doi.org/10.1007/s42102–022–00086–1

19. Z. Yang, C. C. Ma, E. Oterkus, S. Oterkus, K. Naumenko, B. Vazic, Analytical solution of the peridynamic equation of motion for a 2–dimensional rectangular membrane, *J Peridyn Nonlocal Model*, **5** (2023), 375–391. https://doi.org/10.1007/s42102–022–00090–5

20. E. Oterkus, E. Madenci, M. Nemeth, Stress analysis of composite cylindrical shells with an elliptical cutout, *J mech mater struct*, **2** (2007), 695–727.

21. T. Ni, M. Zaccariotto, Q. Z. Zhu, U. Galvanetto, Coupling of FEM and ordinary state–based peridynamics for brittle failure analysis in 3D, *Mech Adv Mater Struc*, **28** (2021), 875–890. https://doi.org/10.1080/15376494.2019.1602237

22. A. Pagani, E. Carrera, Coupling three-dimensional peridynamics and high-order one-dimensional finite elements based on local elasticity for the linear static analysis of solid beams and thin-walled reinforced structures, *Int J Numer Meth Eng*, **121** (2020), 5066–5081. https://doi.org/10.1002/nme.6510

23. Y. Xia, X. Meng, G. Shen, G. Zheng, P. Hu, Isogeometric analysis of cracks with peridynamics, *Comput Method Appl M*, **377** (2021), 113700. https://doi.org/10.1016/j.cma.2021.113700

24. R. Liu, J. Yan, S. Li, Modeling and simulation of ice–water interactions by coupling peridynamics with updated Lagrangian particle hydrodynamics, *Comput. Part. Mech.*, **7** (2020), 241–255. https://doi.org/10.1007/s40571–019–00268–7

25. Y. Wang, X. Zhou, Y. Wang, Y. Shou, A 3–D conjugated bond–pair–based peridynamic formulation for initiation and propagation of cracks in brittle solids, *International Journal of Solids and Structures*, **134** (2018), 89–115. https://doi.org/10.1016/j.ijsolstr.2017.10.022

26. V. Diana, A. Bacigalupo, M. Lepidi, L. Gambarotta, Anisotropic peridynamics for homogenized microstructured materials, *Comput Method Appl M*, **392** (2022), 114704. https://doi.org/10.1016/j.cma.2022.114704

27. Y. Mikata, Peridynamics for fluid mechanics and acoustics, *Acta Mech*, **232** (2021), 3011–3032. https://doi.org/10.1007/s00707–021–02947–0

28. E. Madenci, A. Barut, M. Dorduncu, *Peridynamic differential operator for numerical analysis*, Berlin: Springer International Publishing, 2019, 978–980. https://doi.org/10.1007/978–3–030–02647–9

29. H. Ren, X. Zhuang, T. Rabczuk, A higher order nonlocal operator method for solving partial differential equations, *Comput Method Appl M*, **367** (2020), 113132. https://doi.org/10.1016/j.cma.2020.113132

30. H. Ren, X. Zhuang, T. Rabczuk, A nonlocal operator method for solving partial differential equations, *Comput Method Appl M*, **358** (2020), 112621. https://doi.org/10.1016/j.cma.2019.112621

31. X. Zhuang, H. Ren, T. Rabczuk, Nonlocal operator method for dynamic brittle fracture based on an explicit phase field model, *Eur J Mech A-solid*, **90** (2021), 104380. https://doi.org/10.1016/j.euromechsol.2021.104380

32. Z. Yang, E. Oterkus, S. Oterkus, C. C. Ma, Double horizon peridynamics, *Math Mech Solids*, **28** (2023), 2531–2549. https://doi.org/10.1177/10812865231173686

33. H. Ren, X. Zhuang, Y. Cai, T. Rabczuk, Dual-horizon peridynamics, *International Journal for Numerical Methods in Engineering*, **108** (2016), 1451–1476. https://doi.org/10.1016/j.cma.2016.12.031

34. B. Wang, S. Oterkus, E. Oterkus, Derivation of dual-horizon state-based peridynamics formulation based on Euler-Lagrange equation, *Continuum Mech Therm*, **35** (2023), 841–861. https://doi.org/10.1007/s00161–020–00915–y

35. A. Javili, R. Morasata, E. Oterkus, S. Oterkus, Peridynamics review, *Math Mech Solids*, **24** (2019), 3714–3739. https://doi.org/10.1177/1081286518803411

36. E. Madenci, E. Oterkus, *Peridynamic Theory and Its Applications*, New York: Springer New York, 2013. https://doi.org/10.1007/978–1–4614–8465–3

37. L. Lopez, S. F. Pellegrino, A space-time discretization of a nonlinear peridynamic model on a 2D lamina, *Comput Math Appl*, **116** (2022), 161–175. https://doi.org/10.1016/j.camwa.2021.07.004

38. S. Jafarzadeh, A. Larios, F. Bobaru, Efficient solutions for nonlocal diffusion problems via boundary-adapted spectral methods, *J Peridyn Nonlocal Model*, **2** (2020), 85–110. https://doi.org/10.1007/s42102–019–00026–6